Chapter 2
Time-Resolved Absorption Spectroscopy

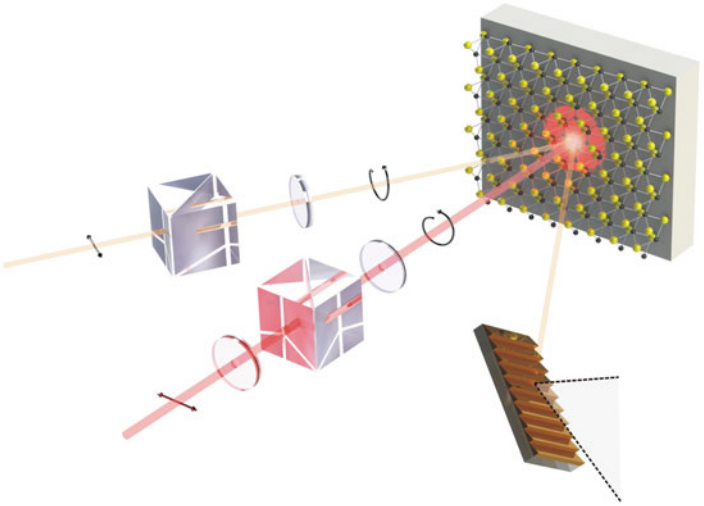

This dissertation work emphasizes on the exciton energy shift that is induced by femtosecond light pulses. At equilibrium, the exciton energy level in monolayer TMDs sits in the visible regime, e.g., $E_0 = 2$ eV in monolayer WS_2. In order to detect this energy shift, we need a broadband probe pulse that is centered in the visible spectrum. White light continuum generation is a nonlinear optical process capable of producing such broadband light pulse between 500 and 700 nm ($\hbar\omega = 1.8 - 2.4$ eV). In this chapter, we will discuss about time-resolved absorption spectroscopy setup (or simply *transient absorption*) that utilizes white light continuum to probe the exciton energy shift in monolayer TMDs. In the first section, we will show the overview of the transient absorption setup. In later sections, we will discuss in more details about (1) laser amplifier, (2) optical parametric amplifier,

E.J. Sie, *Coherent Light-Matter Interactions in Monolayer Transition-Metal Dichalcogenides*, Springer Theses, https://doi.org/10.1007/978-3-319-69554-9_2

and (3) white light continuum generation. Finally, we will discuss about the data analysis based on the optical physics of monolayer materials on a transparent substrate.

2.1 Experimental Setup

2.1.1 Overview

Transient absorption spectroscopy consists of synchronized pump pulses and broadband probe pulses to monitor the pump-induced absorption of materials. Light has three properties, namely, photon energy, polarization, and intensity, that, when tuned precisely, can induce various nonequilibrium phenomena in materials. Examples are resonant excitation of quasiparticles, off-resonance shifting of energy levels, and valley-selective light-matter interaction. For this reason, a transient absorption setup can incorporate different stages of light management area on the optical table to generate light pulses with different photon energies and to control their polarizations and intensities before reaching the sample.

The overview of this transient absorption setup is schematically drawn in Fig. 2.1. In this setup, we use a Ti/sapphire laser amplifier producing laser pulses with duration of 50 fs and at 30 kHz repetition rate. Each pulse is split into two arms. For the pump arm, the pulses are sent to an optical parametric amplifier (OPA) to generate tunable photon energies and modulated by an optical chopper, while for the probe arm, the pulses are sent through a delay stage and a white light continuum generator. The pump and probe polarizations are varied separately by two sets of polarizers and quarter-wave plates, allowing us to perform polarization-dependent measurements, and an additional half-wave plate for tuning the pump pulse intensity. The two beams are focused at the sample, and the probe beam is reflected to a monochromator and a photodiode for lock-in detection. The optical chopper is externally triggered at 7.5 kHz by the 30 kHz laser amplifier. Here, in every optical modulation cycle, two adjacent pump pulses are passed, and the next two adjacent pump pulses are blocked by the optical chopper. By scanning the grating and the delay stage, we are able to measure induced reflection $\Delta R/R$ (hence induced absorption $\Delta\alpha$) as a function of energy and time delay.

2.1.2 Laser Amplifier

One important aspect to consider when setting up a transient absorption setup is the laser pulse energy. White light continuum generation is a nonlinear optical process that requires femtosecond pulse energy of 3–5 μJ when using a transparent nonlinear medium such as a sapphire glass. Although this requirement is easily

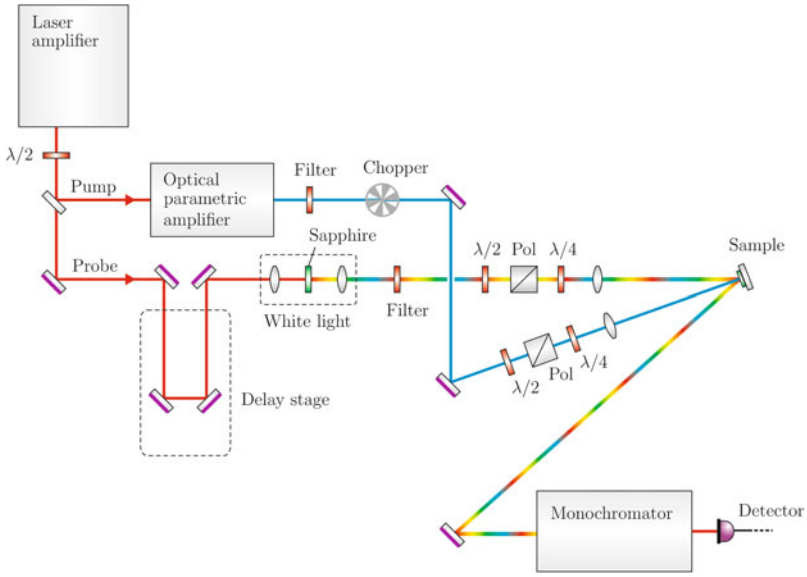

Fig. 2.1 Optical layout of transient absorption spectroscopy setup

managed using a tiny fraction from a laser amplifier's output, it certainly is a huge energy barrier for a laser oscillator. Femtosecond laser amplifiers can produce pulse energy between 10 μJ and 100 mJ, while laser oscillators are limited with pulse energy between 10 and 100 nJ. There is an alternative to generate white light continuum from laser oscillators by using nonlinear photonic crystal fibers. However, laser amplifiers offer more versatile options for transient absorption setup because the remaining pulse energy can be used to generate laser pulses at various wavelengths in the ultraviolet, visible, and mid-infrared using an optical parametric amplifier with typical pulse energy input of 200 uJ.

In our experiment, we use a Ti/sapphire laser amplifier Wyvern 500 from KM Labs and set its repetition rate to 30 kHz. The overview of this amplifier is schematically drawn in Fig. 2.2 and briefly discussed as follows. A mode-locked femtosecond oscillator Griffin (KM Labs) generates laser pulses with pulse duration 50 fs, energy 2 nJ, center wavelength 790 nm, and repetition rate 80 MHz. This oscillator output (seed pulse) is stretched spectrally and temporally to several tens of picoseconds using a pair of diffraction gratings before sent to pulse selection and amplification in gain medium. This technique is called chirped pulse amplification (CPA), and it reduces the peak intensity of the seed pulse to avoid damage to the gain medium through self-focusing and to avoid gain saturation that prevents further amplification. The amplifier uses a cryogenically cooled (−180 °C) gain medium Ti/sapphire single crystal that is optically pumped to achieve population inversion using two external pump laser diodes (Photonics Industries) each with

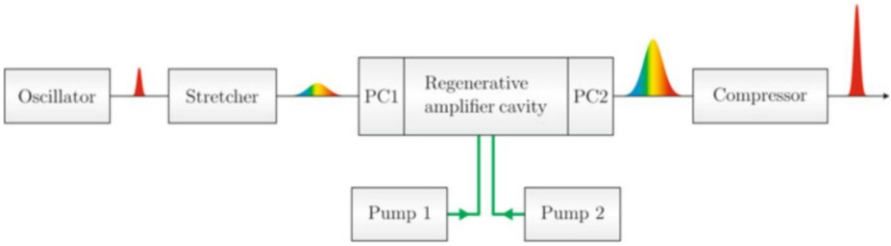

Fig. 2.2 Optical layout inside Wyvern laser amplifier

pulse duration 20 ns (quasi-CW), power 35 W, wavelength 532 nm, and repetition rate 30 kHz (tunable up to 300 kHz).

Regenerative amplifier cavity – The seed polarization is initially perpendicular to the plane of incidence until it passes through an entrance Pockels cell (PC1) to rotate the polarization by $\pi/2$ when activated. The Ti/sapphire crystal is cut at Brewster angle so that a seed pulse that is polarized along the plane of incidence gets trapped in the cavity and amplified. After six to ten passes, the seed pulse is amplified by a factor of 10^6, and an exit Pockels cell (PC2) is activated to rotate the polarization by $\pi/2$ so that the amplified pulse gets reflected from the Brewster's cut surface of the Ti/sapphire crystal and leaves the cavity. The timing of PC1 and PC2 is synchronized with the external laser diodes at 30 kHz, with 80 MHz clock from the oscillator, such that in the time span of 33 μs, only one seed pulse is trapped and amplified.

After exiting the cavity, the amplified pulse is compressed spectrally and temporally using (effectively) a pair of gratings to achieve short pulse duration and very high peak intensity. The Wyvern amplifier output produces pulse duration 50 fs, energy 400 μJ (12 W at best), center wavelength 790 nm, and repetition rate 30 kHz. The laser beam is split by a thin polarizing beam splitter: (1) 230 μJ (7 W) to pump an optical parametric amplifier and (2) 170 μJ is directed toward white light continuum generation (3–5 μJ) where the excess energy is sent to a beam dumper.

2.1.3 Optical Parametric Amplifier

An optical parametric amplifier (OPA) is an optical setup that converts the laser fundamental wavelength into variable wavelengths through parametric amplification process. The principle operation of OPA is based on an optical parametric generation process $\omega_0 = \omega_s + \omega_i$ where one photon of frequency ω_0 (fundamental) is converted into two photons of frequencies ω_s (signal) and ω_i (idler). The output frequencies are varied by tuning the phase-matching condition and time delay between pulses in a nonlinear crystal. In our experiment, we use OPA Palitra from Quantronix that allows tunable wavelengths of signal and idler between 1.1

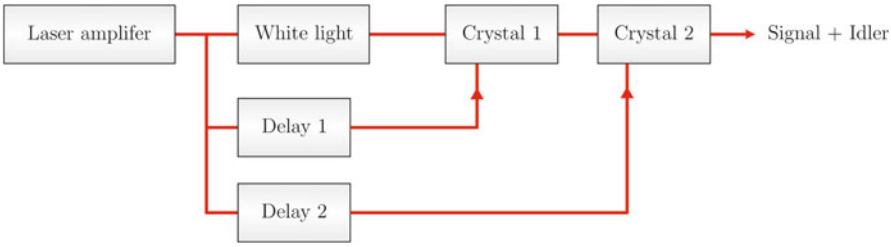

Fig. 2.3 Optical layout inside optical parametric amplifier (OPA)

and 2.5 μm. Longer wavelengths up to 20 μm can be generated inside the OPA through a difference frequency generation (DFG) $\omega_s - \omega_i$, while shorter wavelengths down to 550 nm can be generated outside the OPA through a second harmonic generation (SHG) $2\omega_s$ or $2\omega_i$.

The overview of this OPA is schematically drawn in Fig. 2.3 and briefly discussed as follows. An input laser beam at wavelength 790 nm and pulse energy 230 μJ is split into two beams. About 10% of this beam will be used for the first amplification stage and 90% for the second amplification stage.

In the first amplification stage, the 10% beam is further split into two beams. One beam is used to generate white light continuum in a sapphire glass and directed through a ZnSe substrate to pass only the infrared wing of the continuum and to stretch the beam spectrally and temporally (chirped). This infrared continuum contains the signal frequency component ω_s, and it will be used as a seed pulse. The other beam of frequency ω_0 is directed to a delay stage and used as the pump pulse. The two beams meet at the first nonlinear crystal (Crystal 1) where the optical parametric generation $\omega_0 = \omega_s + \omega_i$ occurs. The output signal and idler frequencies can be tuned by varying the pump pulse time delay (Delay 1) to pick a particular frequency component ω_s from the seed pulse and by rotating the crystal optical axis to achieve a phase-matching condition. The first amplification stage typically produces total pulse energy of 1 μJ (signal and idler).

In the second amplification stage, the amplified beam is directed to the second nonlinear crystal (Crystal 2) and meets the 90% pump beam. Similarly, the amplification efficiency is tuned by varying the second pump delay (Delay 2) and by rotating the crystal axis. This OPA is capable of producing total output energy of 45 μJ (signal + idler) with efficiency of 20% when the idler wavelength is set to 2.1 μm. The output of this OPA is used as the pump pulse in transient absorption setup because it can provide a tunable pump wavelength at high peak intensity.

2.1.4 White Light Continuum

White light continuum generation is a nonlinear optical process that converts laser pulses with narrow spectral bandwidth into pulses with very broad spectral

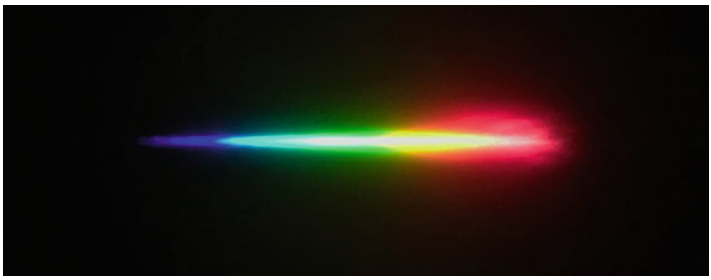

Fig. 2.4 Real image of white light continuum generated in our setup

bandwidth. For instance, in our setup we use a near infrared laser pulse that is focused into a transparent nonlinear medium to generate a visible white beam when projected on the screen (Fig. 2.4). This phenomenon was first observed by R. Alfano and S. Shapiro in 1970 [1]. Such a spectral broadening is driven by the nonlinear effects of self-phase modulation (SPM). This results from the Kerr nonlinearity of materials that also gives rise to Kerr self-focusing. We discuss this briefly as follows. Laser pulses with a Gaussian intensity time profile are given by

$$I(t) = I_0 \exp\left(-\frac{t^2}{\tau^2}\right) \tag{2.1}$$

where I_0 is the peak intensity and τ is the $1/e$ pulse duration (Fig. 2.5a). At high intensity, laser pulses that are traveling inside a medium can induce a refractive index change

$$n(I) = n_0 + n_2 I \tag{2.2}$$

where n_0 is the linear refractive index and n_2 is the nonlinear refractive index due to $\chi^{(3)}$ nonlinearity of the medium. The electric field of an incident laser pulse propagating in vacuum in $\hat{z}$ direction can be expressed as $\mathcal{E}(t) = \mathcal{E}_0 \cos(kz - \omega t)$. The time-varying laser intensity results in a time-varying refractive index of material $n(t)$, leading to a phase shift of the pulse's electric field

$$\phi(t) = \omega_0 t - kz = \omega_0 t - \frac{2\pi n(t)}{\lambda_0} L \tag{2.3}$$

where ω_0 and λ_0 are the carrier frequency and vacuum wavelength of the pulse, and L is the distance the pulse has traveled. The time-varying phase shift results in a time-varying frequency shift of the pulse (Fig. 2.5b), and the instantaneous frequency is given by

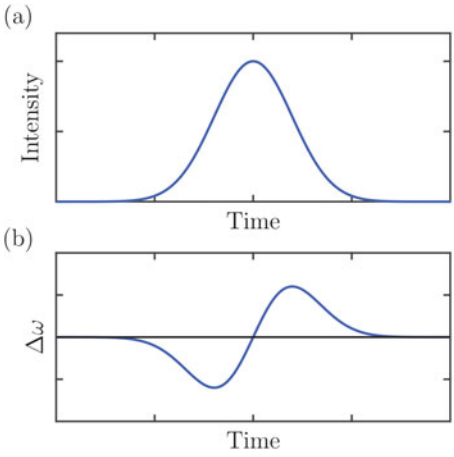

Fig. 2.5 (**a**) Laser pulse with a Gaussian temporal profile. (**b**) Frequency shift due to self-phase modulation after passing through a transparent nonlinear medium

$$\omega(t) = \frac{d\phi(t)}{\mathrm{dt}} = \omega_0 + \left(\frac{4\pi \mathrm{L} n_2 I_0}{\lambda_0 \tau^2}\right) t \exp\left(-\frac{t^2}{\tau^2}\right) \tag{2.4}$$

We can analyze the frequency shifts in three different time segments. The leading edge of the pulse shifts to lower frequencies (red-shifted), the trailing edge shifts to higher frequencies (blue-shifted), while the center exhibits no frequency shift. Although the carrier frequency $\omega(t)$ varies in time, the envelope temporal profile is effectively unchanged. Thus the spectral broadening maintains the incident pulse duration. However, the effect of group velocity dispersion through a transparent medium still occurs. In medium with normal dispersion, the red leading edge of the pulse travels with a faster group velocity, while the blue trailing edge with a slower group velocity. This effect spreads the frequency components temporally, an effect known as *chirp*, which can be as wide as 1 picosecond for wavelength range of 500–700 nm (Fig. 2.6). Nevertheless, the individual packets of frequency components still maintain the femtosecond pulse duration of the incident pulse, which is an important criterion for ultrafast transient absorption experiment.

In the above discussion, we have shown that self-phase modulation in the time domain can result in a white light continuum generation. Meanwhile, self-phase modulation in the spatial domain can also result in a distinct appearance of the white light pattern on the screen. The continuum appears as a round white disk surrounded by a concentric rainbow-like pattern (Fig. 2.7a–d). This is called a *conical emission* and it exhibits a large divergence angle. This is similar to the Kerr self-focusing effect except now we have multiple different wavelengths in the continuum.

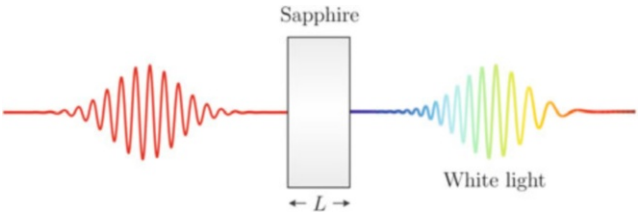

Fig. 2.6 Incoming near IR laser pulse undergoes a self-phase modulation inside a sapphire glass, resulting in an outgoing white light continuum with a linear chirp

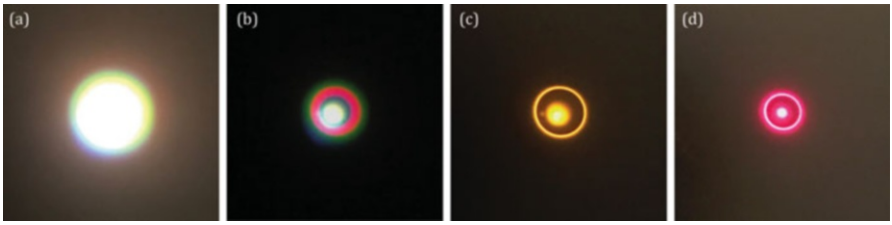

Fig. 2.7 Capturing the conical emission feature. (**a**) Full intensity white light continuum. (**b**) Reduced intensity white light continuum, showing the rainbow-like pattern due to conical emission. (**c**) *Orange* color component after using 590 nm band pass filter. (**d**) *Red color* component after using 660 nm band pass filter

2.2 Data Analysis

Throughout our analysis, we used the proper definitions of reflectance R, transmittance T, and absorptance α, which, respectively, means the fractions of incident electromagnetic power that is reflected, transmitted, and absorbed at the monolayer interface (between vacuum and substrate). This is in contrast to reflectivity and transmittivity, which are technically only valid for semi-infinite system. We also used more familiar names such as absorbance and absorption to mean, quantitatively, the absorptance α of monolayer TMDs.

Pump-probe experiments detect small changes in probe reflectance (or transmittance) that is induced by pump excitation. This gives the differential reflectance $\Delta R/R$ as a function of energy and time delay, from which we can obtain the transient reflectance, $R(t) = R_0(1 + \Delta R(t)/R_0)$, where R_0 is the reflectance of the system in equilibrium. In fact, the absorptance α (or the induced absorptance $\Delta\alpha$) is what we really want (as shown in the main text) because it provides the explicit information about the optical transition matrix element of the system. The absorptance and the reflectance are related through the complex dielectric function $\widetilde{\epsilon}$. This relation can be derived using Maxwell equations shown in Sect. 2.2. We obtain $\widetilde{\epsilon}(\omega, t)$ by fitting $R(\omega, t)$ using a Kramers-Kronig (KK) constrained variational analysis [2] shown in Sect. 2.1. Finally, we construct $\alpha(\omega, t)$ by repeating this

procedure at different time delays. The details of the above procedure are described as follows, in the case for monolayer TMD WS_2.

2.2.1 Kramers-Kronig Analysis

First, we want to find the relation between the complex dielectric function and the optical properties such as reflectance, transmittance, and absorptance by using Maxwell's equations. It is important to include the substrate influence on electromagnetic radiation especially for atomically thin materials. Here, the current density in a monolayer WS_2 sample is described by a delta function, $j_x = \widetilde{\sigma}(\omega)\delta(z)$ E_x where $\widetilde{\sigma}$ is the complex conductivity and E_x is the x-component of the probe electric field (along the sample's surface). By substituting this into Maxwell's equations and using the appropriate boundary conditions between the monolayer and the substrate, we can obtain the reflectance as

$$R(\omega) = \frac{\left(1 - n_s - \frac{\omega d}{c}\epsilon_2\right)^2 + \left(\frac{\omega d}{c}(\epsilon_1 - 1)\right)^2}{\left(1 + n_s + \frac{\omega d}{c}\epsilon_2\right)^2 + \left(\frac{\omega d}{c}(\epsilon_1 - 1)\right)^2} \tag{2.5}$$

and the transmittance as

$$T(\omega) = \frac{4n_s}{\left(1 + n_s + \frac{\omega d}{c}\epsilon_2\right)^2 + \left(\frac{\omega d}{c}(\epsilon_1 - 1)\right)^2} \tag{2.6}$$

where n_s is the substrate's refractive index (1.7675 for sapphire at photon energy of 2.07 eV), d is the effective thickness of the monolayer (0.67 nm), and ϵ_1 and ϵ_2 are the real and imaginary parts of the dielectric function, respectively. Here, the 2D dielectric function is expressed as

$$\widetilde{\epsilon}(\omega) = 1 + \frac{4\pi i\widetilde{\sigma}/d}{\omega} \tag{2.7}$$

Meanwhile, the absorptance can be expressed as

$$\alpha(\omega) = \frac{4\frac{\omega d}{c}\epsilon_2}{\left(1 + n_s + \frac{\omega d}{c}\ \epsilon_2\right)^2 + \left(\frac{\omega d}{c}(\epsilon_1 - 1)\right)^2} \tag{2.8}$$

These expressions are exact, and they are valid for any monolayer materials on a dielectric substrate. We find that the presence of the substrate significantly influences the optical properties of the monolayer WS_2 above it. As compared to an isolated monolayer WS_2, the reflectance is enhanced, while both the transmittance and the absorptance are reduced. In graphene, the above expressions can be further simplified because the real part of its dielectric function is featureless in the visible spectrum ($\epsilon_1 \sim 1$, negligible σ_2). This is, however, not the case for monolayer WS_2,

and we must include both the real and imaginary parts of the dielectric function to obtain accurate results. In situation where none of the equilibrium absorptance, reflectance, or transmittance spectrum is available, the pump-induced absorptance $\Delta\alpha$ can still be estimated from the measured $\Delta R/R$ or $\Delta T/T$ through the following expression:

$$\frac{\Delta R}{R} = \left[\left(\frac{n_s+1}{n_s-1}\right) + \frac{n_s}{(n_s-1)^2}\frac{\left(\gamma_1^2+\gamma_2^2\right)}{\gamma_2}\right]\Delta\alpha \tag{2.9}$$

$$\frac{\Delta T}{T} = -\left[\left(\frac{n_s+1}{2}\right) + \frac{\left(\gamma_1^2+\gamma_2^2\right)}{4\gamma_2}\right]\Delta\alpha \tag{2.10}$$

where ΔR and ΔT are the pump-induced changes of the probe reflectance R and transmittance T, n_s is the refractive index of the substrate, $\gamma_1 = \omega d(\epsilon_1 - 1)/c$, and $\gamma_2 = \omega d\epsilon_2/c$. In situation where γ_1^2 and γ_2^2 are small, such as graphene and few other TMDs, only the first term in the bracket needs be considered.

In our analysis, we used the equilibrium absorptance α of monolayer WS_2 measured using differential reflectance microscopy. The absorptance spectrum contains peaks from the A exciton at 2.0 eV. The equilibrium reflectance R_0 can then be constructed from α by finding the appropriate complex dielectric function $\widetilde{\epsilon}$ as expressed in Eqs. 2.7 and 2.8. To do this, we implemented a Kramers-Kronig (KK) constrained variational analysis [2] to extract $\tilde{\epsilon}$ from the measured α in thin-film approximation. Here, the total dielectric function is constructed by many Drude-Lorentz oscillators, which are anchored at equidistant energy spacing, in the following form

$$\widetilde{\epsilon}(\omega) = \epsilon_\infty + \sum_{k=1}^{N} \frac{\omega_{p,k}^2}{\omega_{0,k}^2 - \omega^2 - i\omega\gamma_k} \tag{2.11}$$

In our calculations, we used $N = 40$ oscillators with a fixed linewidth of $\gamma_k = 50$ meV spanning the energy range of $1.77\,\text{eV} \le \omega_{0,k} \le 2.40\,\text{eV}$, and we found that these parameters can fit α spectrum very well. We can then construct R_0 spectrum by using $\widetilde{\epsilon}$ obtained from the above analysis.

The transient absorptance spectra $\alpha(t)$ can be obtained by performing similar (KK) analysis. This time we inferred the absorptance from the reflectance at different time delays: $R(t) = R_0(1 + \Delta R(t)/R_0)$, where the differential reflectance $\Delta R(t)/R_0$ is measured directly from the experiments.

2.2.2 *Maxwell's Equations for Monolayer Sample*

In this section, we provide a full derivation from Maxwell's equations in order to obtain the exact solutions of reflectance $R(\omega)$, transmittance $T(\omega)$, and absorptance spectra $\alpha(\omega)$ for any monolayer materials on a substrate. Readers who are interested

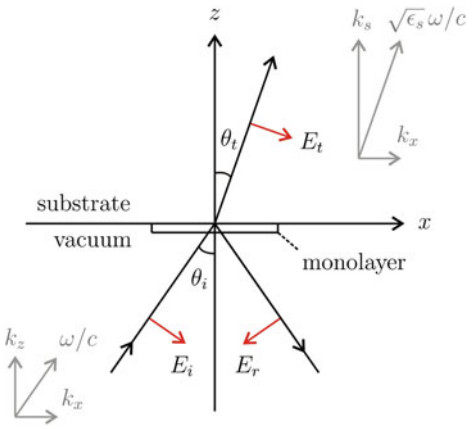

Fig. 2.8 Schematic of the plane of incidence

in this section should also refer to the original articles by L. A. Falkovsky [3] and T. Stauber [4] in the study of graphene. Here, we express the solutions in terms of the complex dielectric function $\widetilde{\epsilon}(\omega)$ or conductivity $\widetilde{\sigma}(\omega)$ for Kramers-Kronig analysis shown in previous section.

The electromagnetic wave equation at frequency ω, inside a medium with a dielectric constant ϵ and a current density $\mathbf{j}$, can be expressed as

$$\nabla(\nabla \cdot \mathbf{E}) - \nabla^2 \mathbf{E} = \epsilon \frac{\omega^2}{c^2} \mathbf{E} + \frac{4\pi i\omega}{c^2} \mathbf{j} \tag{2.12}$$

We consider a situation (Fig. 2.8) where the monolayer medium spreads on the xy plane with a current density $j_x = \widetilde{\sigma}(\omega)\delta(z)E_x(x,t)$ that is driven by a propagating electric field on the xz plane of the form $\mathbf{E} = (E_{0x}, 0, E_{0z})e^{i(\mathbf{k}\cdot\mathbf{r} - \omega t)}$. By evaluating the partial derivatives of $\mathbf{E}$, the two components of the wave equation can be expressed as

$$ik_x \frac{\partial E_z}{\partial z} - \frac{\partial^2 E_x}{\partial z^2} - \epsilon \frac{\omega^2}{c^2} E_x = \frac{4\pi i\omega}{c^2} j_x \tag{2.13}$$

$$ik_x \frac{\partial E_x}{\partial z} + \left(k_x^2 - \epsilon \frac{\omega^2}{c^2}\right) E_z = 0 \tag{2.14}$$

where we have used $\partial/\partial x \rightarrow ik_x$ because the law of refraction requires that k_x is conserved, while K_z is not. Boundary conditions for the tangential and normal components of the field (red arrows) yield

$$E_x = (E_i - E_r)\cos\theta_i = E_t \cos\theta_t \tag{2.15}$$

$$\epsilon_s E_z|_{z=0^+} - E_z|_{z=0^-} = 4\pi \int_{0^-}^{0^+} \rho(z)\mathrm{d}z \tag{2.16}$$

where we have used $\epsilon = \epsilon_s$ for the substrate and $\epsilon = 1$ for the vacuum. The charge density ρ and the current density j_x must satisfy the continuity equation $\partial\rho/\partial t + \nabla \cdot \mathbf{j} = 0$. Since they are driven by the same external field $E_x(x, t)$, we can then obtain a relation

$$\rho = j_x k_x/\omega \tag{2.17}$$

Equation 2.16 can now be evaluated by substituting E_z from Eq. 2.14 and ρ from Eq. 2.17, which yields

$$\frac{\epsilon_s}{k_s^2}\frac{\partial E_x}{\partial z^+} - \frac{1}{k_z^2}\frac{\partial E_x}{\partial z^-} = \frac{4\pi\widetilde{\sigma}}{i\omega}E_x|_{z=0} \tag{2.18}$$

where the relations between k_x, k_z, and k_s are shown in Fig. 2.8. Note that the fields at the boundary are $E_x|_{z^+} = E_t e^{i(k_x x + k_s z)} \cos\theta_t$ and $E_x|_{z^-} = \left(E_i e^{i\mathbf{k}\cdot\mathbf{r}} - E_r e^{-i\mathbf{k}\cdot\mathbf{r}}\right)\cos\theta_i$. Substituting these will yield

$$\left(\frac{\epsilon_s}{k_s} + \frac{4\pi\widetilde{\sigma}}{\omega}\right)E_t \cos\theta_t = \frac{1}{k_z}(E_i + E_r)\cos\theta_i \tag{2.19}$$

$$(E_i - E_r)\cos\theta_i = E_t \cos\theta_t \tag{2.20}$$

These are the two equations that will be used to obtain the reflectance, transmittivity, and absorptance of the monolayer. For convenience, we have moved Eq. 2.15 into 2.20.

At normal incidence, $k_s = \sqrt{\epsilon_s}\omega/c$ and $k_z = \omega/c$; hence the coefficients of amplitude reflection and transmission [5] can be simplified into

$$-r = -\frac{E_r}{E_i} = \frac{1 - n_s - \frac{4\pi\widetilde{\sigma}}{c}}{1 + n_s + \frac{4\pi\widetilde{\sigma}}{c}} \tag{2.21}$$

$$t = \frac{E_t}{E_i} = \frac{2}{1 + n_s + \frac{4\pi\widetilde{\sigma}}{c}} \tag{2.22}$$

where $\widetilde{\sigma} = \sigma_1 + i\sigma_2$ is the complex conductivity of the monolayer, and we have used $\sqrt{\epsilon_s} = n_s$ for an insulating substrate. Finally, we can obtain the reflectance R and the transmittance T, as well as the absorptance α through the energy conservation $|r|^2 + n_s|t|^2 + \alpha = 1$ [5],

$$R = |r|^2 = \frac{\left(1 - n_s - \frac{4\pi\sigma_1}{c}\right)^2 + \left(\frac{4\pi\sigma_2}{c}\right)^2}{\left(1 + n_s + \frac{4\pi\sigma_1}{c}\right)^2 + \left(\frac{4\pi\sigma_2}{c}\right)^2} \tag{2.23}$$

$$T = n_s|t|^2 = \frac{4n_s}{\left(1 + n_s + \frac{4\pi\sigma_1}{c}\right)^2 + \left(\frac{4\pi\sigma_2}{c}\right)^2} \tag{2.24}$$

$$\alpha = \frac{4\left(\frac{4\pi\sigma_1}{c}\right)}{\left(1 + n_s + \frac{4\pi\sigma_1}{c}\right)^2 + \left(\frac{4\pi\sigma_2}{c}\right)^2} \tag{2.25}$$

The obtained $\alpha(\omega)$ is the absorptance of a monolayer medium deposited on an insulating substrate. The whole derivation already accounts for the out-of-phase back-reflected electric field that reduces the light intensity impinging on the monolayer. The above solutions can be expressed in terms of $\widetilde{\epsilon}$ instead of $\widetilde{\sigma}$ using the following relation:

$$\widetilde{\epsilon} = 1 + \frac{4\pi i\widetilde{\sigma}/d}{\omega} \tag{2.26}$$

Note that $\widetilde{\sigma}$ has different units in 2D (here) and in 3D; hence we keep the dielectric function dimensionless by introducing the monolayer thickness d. In order to convert these Gaussian-unit equations into the SI-unit, we can use $4\pi \rightarrow 1/\epsilon_0$ where $\epsilon_0 (= 8.85 \times 10^{-2}\text{F/m})$ is the vacuum permittivity.

References

1. R.R. Alfano, S.L. Shapiro, Observation of self-phase modulation and small-scale filaments in crystals and glasses. Phys. Rev. Lett. **24**, 592–594 (1970)
2. A.B. Kuzmenko, Kramers–Kronig constrained variational analysis of optical spectra. Rev. Sci. Instrum. **76**, 083108 (2005)
3. L.A. Falkovsky, Optical properties of graphene. J. Phys. Conf. Ser. **129**, 012004 (2008)
4. T. Stauber, N.M.R. Peres, A.K. Geim, Optical conductivity of graphene in the visible region of the spectrum. Phys. Rev. B **78**, 085432 (2008)
5. E. Hecht. *Optics*, 4th ed. (Addison-Wesley, 2002)

http://www.springer.com/978-3-319-69553-2

Coherent Light-Matter Interactions in Monolayer Transition-Metal Dichalcogenides

Sie, E.J.

2018, XVII, 129 p. 83 illus., 82 illus. in color., Hardcover
ISBN: 978-3-319-69553-2